NÖHÜ Müh. Bilim. Derg. / NOHU J. Eng. Sci., 2024; 13(3), 969-974

Niğde Ömer Halisdemir Üniversitesi Mühendislik Bilimleri Dergisi
Niğde Ömer Halisdemir University Journal of Engineering Sciences

Araştırma makalesi / Research article

www.dergipark.org.tr/tr/pub/ngumuh / www.dergipark.org.tr/en/pub/ngumuh

Computational fluid dynamics simulation of Reynolds stress frequencies in the FDA nozzle

FDA nozulundaki Reynolds gerilme frekanslarının hesaplamalı akışkanlar dinamiği simülasyonu

Mesude Avcı[1,*]

[1] *Cumhuriyet University, Department of Chemical Engineering, 58140, Sivas Türkiye*

Abstract

It is known that examining turbulence effects on medical devices has an important effect in design and optimization of blood-contacting devices. CFD has been commonly used on prosthetic heart valves, stents, and Ventricular Assist Devices (VADs) in both the design process and also on hemodynamics of the flow characteristics. In this study, flows in the FDA nozzle were modeled to examine Reynolds stresses in the whole domain. The flow behavior was determined by applying the Reynolds-Averaged Navier-Stokes model of turbulence (k-ω SST) to simulate five distinctive experimental cases in the nozzle taken from the literature. The Reynolds stress frequencies are determined for the five different experimental conditions. Results showed that the highest velocity case (corresponding throat Reynolds number of 6500) has much higher Reynolds stresses with a high number of frequencies. However, the lowest velocity case has very small Reynolds numbers in a very high frequency. When different parts of the nozzle were examined, the Reynolds stress values showed more fluctuations for the higher velocities and more regular profiles for the lower velocity cases.

Keywords: Computational fluid dynamics, Hemolysis, Artificial organs, Ventricular assist devices, Turbulence, Reynolds stresses

Öz

Tıbbi cihazlar üzerindeki türbülans etkilerinin incelenmesinin, kanla temas eden cihazların tasarımında ve optimizasyonunda önemli bir etkiye sahip olduğu bilinmektedir. Hesaplamalı Akışkanlar Mekaniği (HAD), protez kalp kapakçıkları, stentler ve Ventriküler Destek Cihazları (VAD) üzerinde hem tasarım sürecinde hem de akış karakteristiklerinin hemodinamiği üzerinde yaygın olarak kullanılmaktadır. Bu çalışmada, The U.S. Food and Administration (FDA) nozulundaki akışlar modellenerek tüm etki alanındaki Reynolds gerilmeleri incelenmiştir. Akış davranışı, literatürden alınan nozüldeki beş farklı deneysel vakayı simüle etmek için Reynolds Ortalamalı Navier-Stokes türbülans modeli (k-ω SST) uygulanarak belirlenmiştir. Beş farklı deneysel durum için Reynolds gerilme frekansları belirlenmiştir. Sonuçlar, en yüksek hız durumunun (6500, boğaz Reynolds sayısına karşılık gelir) yüksek frekans sayısı ile çok daha yüksek Reynols gerilmelerine sahip olduğunu göstermiştir. Bununla birlikte, en düşük hız durumu çok yüksek frekanslarda çok küçük Reynolds sayılarına sahiptir. Nozulun farklı kısımları incelendiğinde, Reynolds gerilme değerleri yüksek hızlar için daha fazla dalgalanma gösterirken, düşük hız durumları için daha düzenli profiller göstermektedir.

Anahtar kelimeler: Hesaplamalı akışkanlar dinamiği, Hemoliz, Yapay organlar, Yardımcı destek cihazları, Turbulans, Reynolds gerilmeleri

1 Introduction

Artificial hearts and Ventricular Assist Devices (VADs) have been widely used with the improvement of technology and increased life expectancy [1]. However, the procedure of advancement and analysis in design of such devices is both costly and time-consuming. Therefore, numerical tools such as Computational Fluid Dynamics (CFD) have been commonly used to develop, analyze and optimize VADs [2-9], stents [10-12], and prosthetic heart valves [13-16]. CFD effectively enhances the evolution process of these devices and supplies specific information on physical quantities that are difficult to measure experimentally.

Moreover, CFD can not only serve in the design process of medical devices but also can examine the alterations in the hemodynamic environment such as the alteration of blood flow dynamics and/or the fluid forces exerted on the device. It is significant that CFD precisely resolves the flow characteristics in medical devices by predicting both mean quantities and instantaneous quantities such as turbulence, which is an important consideration for examining cardiovascular flows [17-19], predicting hemolysis and thrombosis [20-25].

The U.S. Food and Drug Administration (FDA) developed a benchmark nozzle model that consists of a conical shape at one end of the throat and a sudden expansion at the other end to validate innovative biomedical CFD methodologies. For that purpose, this nozzle was developed to have flow behaviors that could closely mirror those in medical devices such as flow expansion and contraction,

* Corresponding author, e-posta / e-mail: mesude@cumhuriyet.edu.tr (M. Avcı)
Geliş / Recieved: 05.04.2024 Kabul / Accepted: 31.05.2024 Yayımlanma / Published: 15.07.2024
doi: 10.28948/ngumuh.1465806

local high shear stresses, and flow recirculation. This device is especially impressive and challenging from a numerical perspective because it has been designed in a way that all flow types of laminar, transitional, and turbulent flows, which is very common in medical devices, [26-28], are covered.

Reynolds stress estimation in CFD is important for accurately predicting flow behavior, particularly in complex geometries like the FDA Nozzle. The Reynolds stress means turbulent fluctuations in the flow field and is critical for capturing the effects of turbulence on the flow. Different studies have highlighted the significance of Reynolds stress calculations in CFD simulations of the FDA Nozzle. Manchester et al. [29] used large-eddy simulations (LES) in the FDA nozzle and calculated the Reynolds (Re) stresses only for the transitional flow condition (Re=2000). They found good agreement between the experimental data and their results in the jet breakdown regions. However, they observed up to 4% to 20% difference near the jet core. Taylor et al. [24], used two flow conditions to create laser Doppler velocimetry (LDV) data. They compared axial velocities and viscous stresses to experimental data. The results showed that near the wall in the nozzle throat and in the jet, velocity gradients were high. Dresar et al. [30], modeled the flow condition of Re=6500 by using the Hybrid RANS-LES model. The results showed that the model did not produce enough unsteadiness.

Reynolds stress calculation in CFD simulations of the FDA Nozzle is crucial for accurately predicting flow behavior, especially in turbulent flows. Studies have shown that neglecting Reynolds stresses or relying solely on certain turbulence models can lead to inaccuracies in predicting flow parameters and their effects on biological processes like hemolysis. Therefore, incorporating Reynolds stress calculations in CFD models is essential for improving the accuracy of simulations in complex geometries like the FDA Nozzle.

In this work, a detailed examination of Reynolds stresses applying CFD for the FDA nozzle at five different flow conditions has been carried out. A detailed examination of the model was performed. Background info is discussed in Part 1 and the model details operated for the current examination and also for the computational approach are shown in Part 2. In Part 3, the findings of this work. It is observed that for different parts of the nozzle, the distribution of Reynolds stresses was changing at different flow conditions.

2 Material and method

2.1 Nozzle geometry

The FDA nozzle geometry is shown in Figure 1a. The design of the nozzle was done to have transitional and turbulent flows, faster and slower blood flows by the progressive and rapid differences in the geometry, which is similar to flow behaviors of medical devices [31], [32].

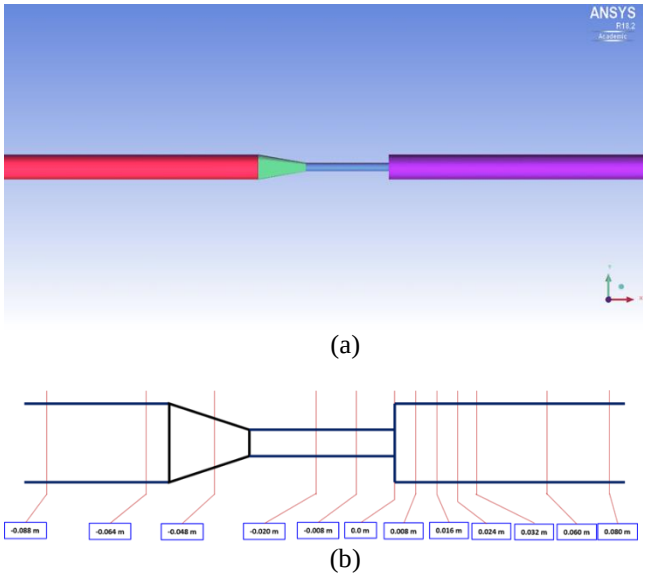

Figure 1. (a) Schematic of FDA nozzle model, flow direction is from left to right; (b) x-position of cross-sectional cuts in the nozzle.

The details of the dimensions were taken from the original experimental data of Stewart et al. [32]. The nozzle geometry contains a straight tube with a diameter (D) of 12 mm, a conical part that decreases the tube diameter to 4 mm when it comes to the throat part then a small straightforward throat part with a length of 40 mm, after that the geometry ends with a rapid escalation with the tube diameter of 12 mm. The inlet and the outlet tube lengths were not specified in the experimental data; they were left for the modeler to decide. The lengths were taken to be 100 times D to be certain about neglecting the entrance effects. The cross-sectional cuts, as shown in Figure 1b, were created in the whole domain for post-processing the results. The flow was simulated using blood with a density of 1040 kg/m^3 and a viscosity of 0.00421 Pa.s.

2.2 Computational grid

The nozzle was meshed using Ansys Fluent 18.2 and its subprogram ICEM CFD (Ansys, Pittsburgh, PA, USA). After a three-dimensional model of the complete domain with the gradual and sudden changes was remodeled, the full geometry was meshed with hexahedral elements. Furthermore, o-grid meshes were used around the inlet and outlet regions to increase the grid characteristics. Subsequent to the grid application to the nozzle, the model was imported into Fluent to run the program and to solve the incompressible Navier-Stokes equations. A grid-independent analysis was performed by refining the mesh in high-velocity regions. The mesh independence analysis results for mean velocity magnitude are illustrated in Figure 2 for the 0.008 m cross-sectional cut. The coarse mesh includes 1854057 cells and 1900860 nodes while the finest mesh has 2592837 cells and 2807657 nodes.

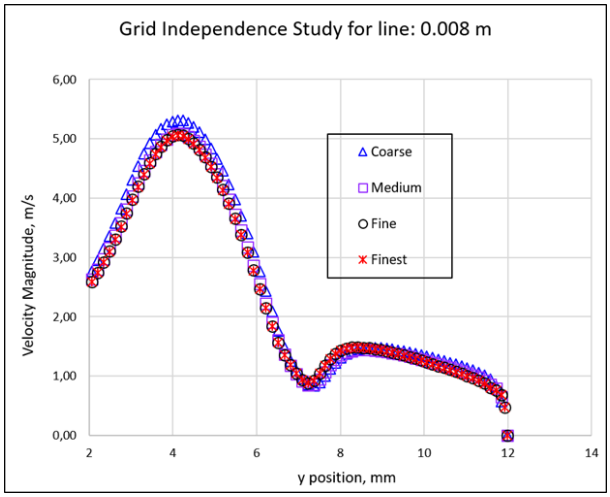

Figure 2. Grid independence analysis for the nozzle for the throat Reynolds number of 500 experiment using the k-ω SST model.

Figure 2 shows that velocity data did not depend on the grid size. The latest grid applied for the FDA nozzle includes 2592837 cells and 2807657 nodes.

2.3 Flow simulation

Modeling the nozzle equipment geometry and solving the governing equations in the whole flow are performed by using the finite volume-based Fluent simulator. The computation procedure started with the lowest velocity (0.05 m/s) which gives the minimum throat Reynolds number applied in the experiments, and after that continuously incrementing the flow velocity up to the stated experimental throat Reynolds number value [32]. The flow modeling was achieved with velocities growing from 0.05 m/s to 0.6 m/s (gives the throat Reynolds numbers of 500 to 6500). The turbulence k-ω SST model was used for the entire nozzle simulations.

The flow rates were named as V_1, V_2, V_3, V_4, and V_5. The throat Reynolds numbers, flow rate, and average inlet velocity values are presented in Table 1.

Tablo 1. Simulation conditions for the FDA nozzle

Experimental Conditions	Thorat Re Number	Flow Rate (m^3/s)	Average Inlet Velocity (m/s)
V_1	500	$5.22*10^{-6}$	0.05
V_2	2000	$2.08*10^{-5}$	0.18
V_3	3500	$3.65*10^{-5}$	0.32
V_4	5000	$5.21*10^{-5}$	0.46
V_5	6500	$6.77*10^{-5}$	0.60

The specified boundary conditions in Fluent for the nozzle were given as velocity inlet at the domain inlet and the no-slip boundary condition on the walls. Fluid flow is assumed to be incompressible and steady. Moreover, a second-order accurate SIMPLE (Semi-implicit Method for Pressure Linked Equation) algorithm is utilized for the pressure-velocity coupling and the second-order upwind scheme is used to discretize the pressure and momentum equations.

3 Results and discussion

3.1 Reynolds stress frequencies in the nozzle

Simulations were completed for the nozzle experiments as illustrated in Table 1. For the lowest throat Reynolds number 500, the Reynolds stresses were determined in the whole domain. After that, the histograms were produced as illustrated in Figure 3.

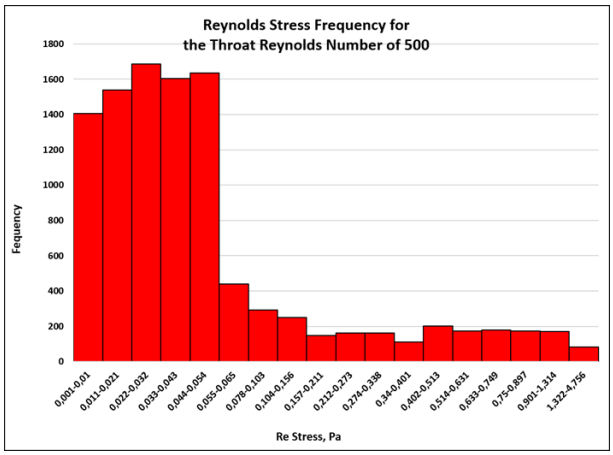

Figure 3. Frequency of Reynolds stresses in the nozzle for the case of the throat Reynolds number of 500.

Figure 3 shows that when the Reynolds stress values are examined in the whole device, the values are mostly near zero. They are changing from 0.001 to 4.756. Moreover, much of the frequency is observed around smaller values or Reynolds numbers. The next flow condition analysed is the condition where the throat Reynolds number is 2000 as can be seen in Figure 4.

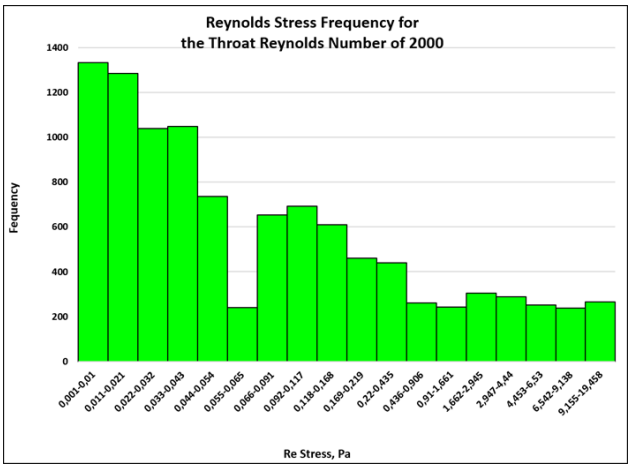

Figure 4. Frequency of Reynolds stresses in the nozzle for the case of the throat Reynolds number of 2000.

Figure 4 illustrates that the Reynolds stress values are still lower values but when compared to 500 cases, the Reynolds stress values are increased. The values are changing from 0.001 to 19.458. Moreover, as shown in the

frequency, they are shifted toward higher values. The experimental condition for the flow condition of throat Reynolds number 3500 is also analyzed and shown in Figure 5.

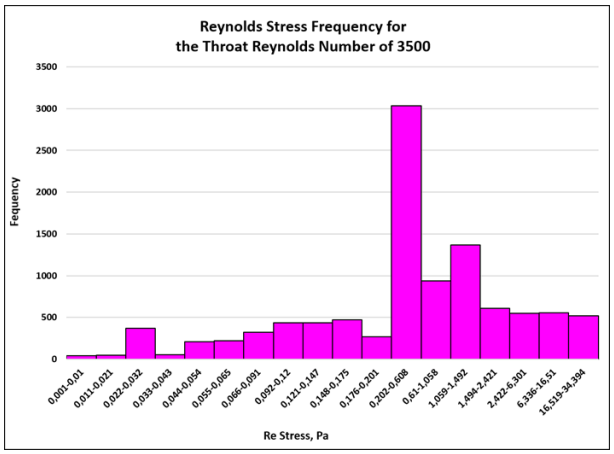

Figure 5. Frequency of Reynolds stresses in the nozzle for the case of the throat Reynolds number of 3500.

Figure 5 shows that the Reynolds stress values are getting higher values when compared to the cases of the throat Reynolds numbers of 500 and 2000 cases. The Reynolds stress values increased up to 34394 Pa. The last experimental condition where the throat Reynolds number is 6500 is also examined as shown in Figure 6.

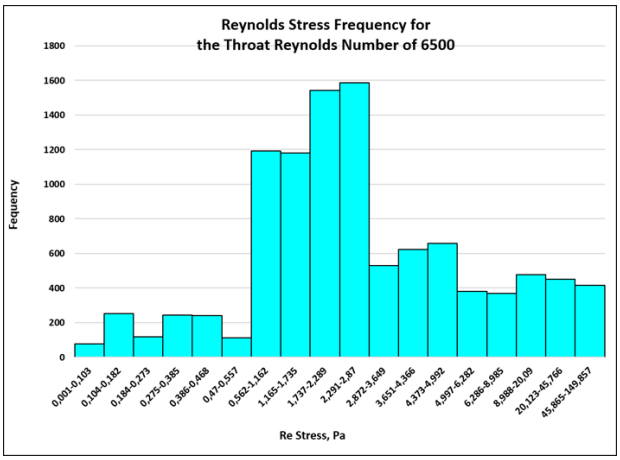

Figure 6. Frequency of Reynolds stresses in the nozzle for the case of the throat Reynolds number of 6500.

As shown in Figure 6, the highest velocity condition which corresponds to the throat Reynolds number of 6500, has the highest Reynolds stress values as expected. The max Reynolds stress value goes to 149857 Pa.

3.2 Reynolds stress values from wall to wall in the nozzle

In addition to the Reynolds stress frequencies, the Reynolds stress values are also determined in the FDA nozzle for different parts. To get a more detailed analysis, the FDA nozzle was divided into 4 different parts as shown in Figure 7.

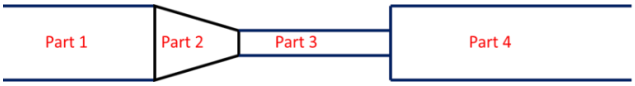

Figure 7. Different parts of the FDA nozzle are used for Reynolds stress values from wall to wall.

For different parts of the nozzle, the Reynolds stress values from wall to wall are examined and shown in Figure 8 and Figure 9,

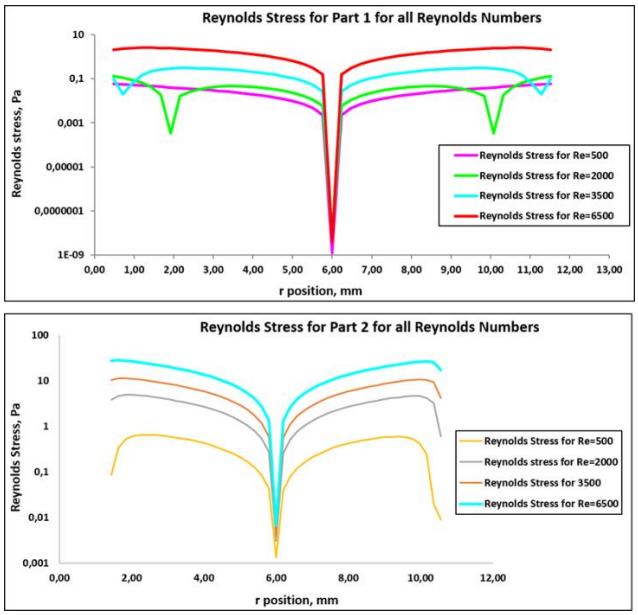

Figure 8. Reynolds stress values for part 1 and part 2 of the FDA nozzle used for Reynolds stress values from wall to wall. The top image is for part 1 and the below one is for part 2.

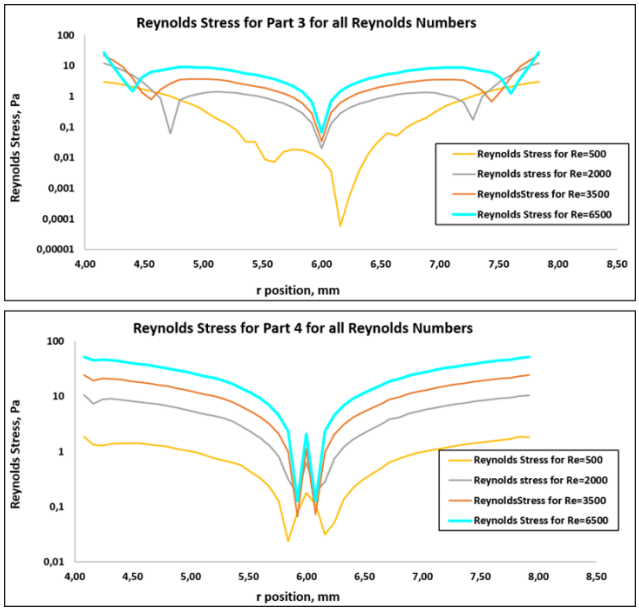

Figure 9. Reynolds stress values for part 3 and part 4 of the FDA nozzle used for Reynolds stress values from wall to wall. The top image is for part 3 and the below one is for part 4.

When the Reynolds stress values are compared for all different parts of the nozzle; Reynolds stresses are mostly constant and then show a sharp decrease around the center of the nozzle for part 1 and part 2. Reynolds stress values show more fluctuations near the center for parts 3 and part 4.

4 Conclusions

CFD is a powerful tool for designing medical devices and also examining flow characteristics such as turbulence on them. It has been known that turbulence has an important effect on the flow behavior of blood-contacting medical devices. Therefore, examining the Reynolds stresses in the FDA nozzle has an essential role clinically since the nozzle has very similar flow behaviors to medical devices. In this work, Reynolds stress calculations were performed in detail which shows the Reynolds stress frequencies in the FDA nozzle. It has been seen that the highest velocity case (corresponds to throat Reynolds number of 6500) has much higher Reynolds stresses with a high number of frequencies. However, the lowest velocity case has very small Reynolds numbers in very high frequencies. When different parts of the nozzle were examined, the Reynolds stress values showed more fluctuations for the higher velocities and more regular profiles for the lower velocity cases.

Conflict of Interest

There is no conflict of interest.

Similarity (iThenticate): %13

References

[1] V. Laxmi, Medical devices: technologies and global markets. BCC Res., 2018.

[2] G. W. Burgreen, J. F. Antaki, Z. J. Wu, and A. J. Holmes, Computational fluid dynamics as a development tool for rotary blood pumps. Artif. Organs, vol. 25, no. 5, pp. 336–340, 2001. doi: 10.1046/j.1525-1594.2001.025005336.x.

[3] K. H. Fraser, T. Zhang, M. E. Taskin, B. P. Griffith, and Z. J. Wu, A quantitative comparison of mechanical blood damage parameters in Rotary Ventricular Assist Devices: shear stress, exposure time, and hemolysis index. J. Biomech. Eng., vol. 134, no. 8, p. 81002, 2012. DOI:10.1115/1.4007092

[4] V. Izraelev et al., A passively suspended Tesla pump left ventricular assist device. ASAIO J., vol. 55, no. 6, pp. 556–561, 2009. doi: 10.1097/MAT.0b013e3181bae73e

[5] Y. S. Morsi, W. Yang, P. J. Witt, A. M. Ahmed, and M. Umezu, Numerical analysis of the flow characteristics of the rotary blood pump. J. Artif. Organs, vol. 4, no. 1, pp. 54–60, 2001, doi: 10.1007/BF01235837.

[6] V.-T. Nguyen et al., Experimentally Validated Hemodynamics Simulations of Mechanical Heart Valves in Three Dimensions. Cardiovasc. Eng. Technol., vol. 3, no. 1, pp. 88–100, 2012, doi: 10.1007/s13239-011-0077-z.

[7] J. Wu, B. E. Paden, H. S. Borovetz, and J. F. Antaki, Computational fluid dynamics analysis of blade tip clearances on hemodynamic performance and blood damage in a centrifugal ventricular assist device. Artif. Organs, vol. 34, no. 5, pp. 402–411, 2010. doi: 10.1111/j.1525-1594.2009.00875.x

[8] C. C. Long, A. L. Marsden, and Y. Bazilevs, Shape optimization of pulsatile ventricular assist devices using FSI to minimize thrombotic risk. Comput. Mech., vol. 54, no. 4, pp. 921–932, 2014, doi: 10.1007/s00466-013-0967-z.

[9] G. A. Giridharan et al., Performance evaluation of a pediatric viscous impeller pump for Fontan cavopulmonary assist. J. Thorac. Cardiovasc. Surg., vol. 145, no. 1, pp. 249–257, Jan. 2013, doi: 10.1016/j.jtcvs.2012.01.082.

[10] C. Karmonik, J. Bismuth, M. G. Davies, D. J. Shah, H. K. Younes, and A. B. Lumsden, A computational fluid dynamics study pre- and post-stent graft placement in an acute type B aortic dissection. Vasc. Endovascular Surg., vol. 45, no. 2, pp. 157–164, Feb. 2011, doi: 10.1177/1538574410389342.

[11] Y. He, N. Duraiswamy, A. O. Frank, and J. E. J. Moore, Blood flow in stented arteries: a parametric comparison of strut design patterns in three dimensions. J. Biomech. Eng., vol. 127, no. 4, pp. 637–647, Aug. 2005, doi: 10.1115/1.1934122.

[12] S. Seshadhri, G. Janiga, O. Beuing, M. Skalej, and D. Thévenin, Impact of Stents and Flow Diverters on Hemodynamics in Idealized Aneurysm Models. J. Biomech. Eng., vol. 133, p. 71005, 2011, doi: 10.1115/1.4004410.

[13] Z. Cheng et al., Assessment of Hemodynamic Conditions in the Aorta Following Root Replacement with Composite Valve-Conduit Graft. Ann. Biomed. Eng., vol. 44, no. 5, pp. 1392–1404, May 2016, doi: 10.1007/s10439-015-1453-x.

[14] I. Borazjani, L. Ge, and F. Sotiropoulos, High-resolution fluid-structure interaction simulations of flow through a bi-leaflet mechanical heart valve in an anatomic aorta. Ann. Biomed. Eng., vol. 38, no. 2, pp. 326–344, Feb. 2010, doi: 10.1007/s10439-009-9807-x.

[15] E. Sirois and W. Sun, Computational Evaluation of Platelet Activation Induced by a Bioprosthetic Heart Valve. Artif. Organs, vol. 35, no. 2, pp. 157–165, Feb. 2011, doi: https://doi.org/10.1111/j.1525-1594.2010.01048.x.

[16] S. Pirola et al., Computational study of aortic hemodynamics for patients with an abnormal aortic valve: The importance of secondary flow at the ascending aorta inlet. APL Bioeng., vol. 2, no. 2, p. 26101, Jun. 2018, doi: 10.1063/1.5011960.

[17] N. Franck, C. Chnafa, J. Sigüenza, V. Zmijanovic, and S. Mendez, Large-Eddy Simulation of Turbulence in Cardiovascular Flows. in Lecture Notes in Applied and Computational Mechanics, 2017, pp. 147–167. doi: 10.1007/978-3-319-59548-1_9.

[18] J. Lantz, T. Ebbers, J. Engvall, and M. Karlsson, Numerical and experimental assessment of turbulent kinetic energy in an aortic coarctation. J. Biomech., vol. 46, no. 11, pp. 1851–1858, 2013, doi: https://doi.org/10.1016/j.jbiomech.2013.04.028.

[19] M. Andersson, J. Lantz, T. Ebbers, and M. Karlsson, Quantitative Assessment of Turbulence and Flow Eccentricity in an Aortic Coarctation: Impact of Virtual Interventions. Cardiovasc. Eng. Technol., vol. 6, no. 3, pp. 281–293, Sep. 2015, doi: 10.1007/s13239-015-0218-x.

[20] A. M. Sallam and N. H. C. Hwang, Human red blood cell hemolysis in a turbulent shear flow: contribution of Reynolds shear stresses. Biorheology, vol. 21, no. 6, pp. 783–797, 1984. doi: 10.3233/bir-1984-21605

[21] M. Grigioni, C. Daniele, G. D'Avenio, and V. Barbaro, A discussion on the threshold limit for hemolysis related to Reynolds shear stress. J. Biomech., vol. 32, no. 10, pp. 1107–1112, 1999. doi: 10.1016/s0021-9290(99)00063-9.

[22] M. V Kameneva, G. W. Burgreen, K. Kono, B. Repko, J. F. Antaki, and M. Umezu, Effects of Turbulent Stresses upon Mechanical Hemolysis: Experimental and Computational Analysis. ASAIO J., vol. 50, no. 5, pp. 418–423, 2004.

[23] S. J. Hund, J. F. Antaki, and M. Massoudi, On the Representation of Turbulent Stresses for Computing Blood Damage. Int. J. Eng. Sci., vol. 48, no. 11, pp. 1325–1331, 2010. doi: 10.1016/j.ijengsci.2010.09.003

[24] J. Taylor et al., Analysis of Transitional and Turbulent Flow Through the FDA Benchmark Nozzle Model Using Laser Doppler Velocimetry. Cardiovasc. Eng. Technol., vol. 7, Jun. 2016, doi: 10.1007/s13239-016-0270-1.

[25] M. Ozturk, E. A. O'Rear, and D. V. Papavassiliou, Hemolysis Related to Turbulent Eddy Size Distributions Using Comparisons of Experiments to Computations. Artif. Organs, vol. 39, no. 12, pp. E227–E239, 2015, doi: 10.1111/aor.12572.

[26] P. Hariharan et al., Multilaboratory particle image velocimetry analysis of the FDA benchmark nozzle model to support validation of computational fluid dynamics simulations. J. Biomech. Eng., vol. 133, no. 4, p. 41002, Apr. 2011, doi: 10.1115/1.4003440.

[27] N. Fehn, W. A. Wall, and M. Kronbichler, Modern discontinuous Galerkin methods for the simulation of transitional and turbulent flows in biomedical engineering: A comprehensive LES study of the FDA benchmark nozzle model. Int. j. numer. method. biomed. eng., vol. 35, no. 12, p. e3228, Dec. 2019, doi: https://doi.org/10.1002/cnm.3228.

[28] N. Sánchez Abad, R. Vinuesa, P. Schlatter, M. Andersson, and M. Karlsson, Simulation strategies for the Food and Drug Administration nozzle using Nek5000. AIP Adv., vol. 10, no. 2, p. 25033, Feb. 2020, doi: 10.1063/1.5142703.

[29] E. L. Manchester and X. Y. Xu, The effect of turbulence on transitional flow in the FDA's benchmark nozzle model using large-eddy simulation. Int. j. numer. method. biomed. eng., vol. 36, no. 10, p. e3389, Oct. 2020, doi: https://doi.org/10.1002/cnm.3389.

[30] P. Drešar and J. Duhovnik, A Hybrid RANS-LES Computational Fluid Dynamics Simulation of an FDA Medical device benchmark. Mechanics, vol. 25, pp. 291–298, Aug. 2019, doi: 10.5755/j01.mech.25.4.20105.

[31] R. A. Malinauskas et al., FDA Benchmark Medical Device Flow Models for CFD Validation. ASAIO J., vol. 63, no. 2, pp. 150–160, 2017, doi: 10.1097/MAT.0000000000000499.

[32] S. F. C. Stewart et al., Assessment of CFD Performance in Simulations of an Idealized Medical Device: Results of FDA's First Computational Interlaboratory Study. Cardiovasc. Eng. Technol., vol. 3, no. 2, pp. 139–160, 2012, doi: 10.1007/s13239-012-0087-5.